Proceedings of the
Annual Stability Conference
Structural Stability Research Council
Atlanta, Georgia, April 21-24, 2026

Compression buckling strength of steel gusset plate in truss bridge connections

Zannatul Mawa Dalia[1], Anjan Bhowmick[2]

Abstract

In steel truss bridges, gusset plates are essential structural components that facilitate the transfer of loads between the connecting members. The collapse of the I-35W Bridge in 2007 brought attention to design flaws in gusset plates. As a result, the Federal Highway Administration conducted further research, leading to the development of the current AASHTO provisions for the design and evaluation of gusset plates in truss bridges. According to AASHTO, the buckling resistance of gusset plates is influenced by both the Whitmore buckling resistance and partial shear yielding around the compression members. While the current limit states may be suitable for intermediate gusset plate connections when two diagonal members are joined, they may be overly conservative for corner gusset plates in through-truss bridges, which could result in unnecessary rehabilitation. Research on the compression buckling behaviour of corner gusset plates in steel through-truss bridges is limited. This study investigates the compression behaviour of gusset plates in steel truss bridges using detailed nonlinear finite element (FE) analysis. The FE models account for both material and geometric nonlinearities while simulating realistic boundary conditions and member interactions. Five gusset plate connections are modelled using ABAQUS and validated against experimental results from the existing literature; three representative models are presented in this paper. A series of corner gusset plate connections in truss bridges is modelled and analysed to investigate their behaviour under compression. The compressive strength derived from detailed FE analyses is then compared with the capacities predicted by AASHTO and CSA S6 standards.

1. Introduction

Gusset plates are crucial components of steel truss bridges, connecting several members and ensuring that forces are distributed safely through the structure. Their performance directly influences the overall stability and redundancy of the bridge system. Following a number of historical failures, most notably the collapse of the I-35W Bridge, when insufficient gusset capacity led to disastrous outcomes, the significance of appropriate gusset plate behaviour became particularly clear (NTSB 2008). As a result, gusset plate behaviour and design have been the subject of in-depth study and ongoing design specification improvement.

[1] Graduate Research Assistant, Concordia University, <zannatdaliace09@gmail.com>
[2] Associate Professor, Concordia University, <anjan.bhowmick@concordia.ca>

The majority of current research has been on interior panel-zone gusset plates, where load pathways are more consistent, and member framing is more symmetrical. Well-known ideas like Whitmore's effective width (Whitmore 1952) and Thornton's column-type buckling formulations (Thornton 1984) have been extensively used for these joints. The present AASHTO (AASHTO 2020) and CSA S6 provisions (CSA S6 2019) are based on these techniques.

Following the I-35W bridge collapse in 2007, gusset plate behaviour received renewed attention, leading to a broad set of analytical, numerical, and experimental investigations. Berman et al. (2012) developed a rapid FE-based assessment approach and recommended revising FHWA's buckling capacity procedure (FHWA 2009) using the modified Thornton method with K = 1.0, where K is the effective length factor used to estimate the buckling length of the Whitmore section. Their results highlighted that common evaluation practices can underestimate capacity for certain joint geometries.

Higgins et al. (2013) tested six full-scale gusset plate specimens specifically targeting sway-buckling behaviour, showing that FHWA's assumed K = 1.2 overestimated effective length, leading to an overly conservative prediction. They reported considerably smaller experimental K-values, suggesting that current assumptions employed for evaluating out-of-plane instability may be excessively conservative and deserve reconsideration.

The compressive capacity of truss-bridge gusset plates was thoroughly investigated experimentally and numerically by Kim et al. (2013), taking into account differences in plate thickness, chamfering, connection length, free-edge distance, and fastener configurations. Their FE modelling approach was validated by full-scale experiments. The impact of chamfering at the compression-diagonal end was a major area of study since chamfers alter the load transfer region and decrease the Whitmore width. To address these effects, the authors proposed two design methods: (i) Method 1, using the full Whitmore width (truncated at free edges) with checks for column-type buckling and partial shear-plane yielding; and (ii) Method 2, using a truncated Whitmore width with a simplified column analogy based on fastener-line spacing.

Crosti and Duthinh (2014) expanded this understanding by analysing the effects of initial out-of-plane imperfections, framing-member stiffness, load sharing among connected members, and load eccentricity. Their FE models, which were validated against available test data, confirmed that FHWA's post-collapse guidelines remain conservative for plates under in-plane compression, even with imperfections approaching one plate thickness.

More recently, Duan and Vinayagamoorthy (2023) introduced the Two-Strut Buckling (TSB) model as an enhanced analytical approach for determining the compressive capacity of gusset plates. Their study was motivated by the observation that several evaluation methods in the AASHTO Manual for Bridge Evaluation, such as the Whitmore section check, the Partial Plane Shear Yielding (PPSY) method, the Basic Corner Check (BCC), and the Truncated Whitmore Section (TWS), often produce inconsistent or overly conservative estimates when applied to compression diagonal gusset plates. Using 116 full-scale tests and refined FE analyses, the authors showed that some of the existing methods can underestimate capacity by 25 to 40%. Their findings highlight the limitations of current evaluation procedures and the need for models that better reflect the mechanics of actual gusset plates.

Current design provisions for gusset plate compression in steel truss bridges are primarily based on simplified assumptions that treat the plate as a column-type member whose effective width and buckling length must be determined indirectly. Current AASHTO provisions estimate compressive resistance by applying the Whitmore effective width combined with a column-type buckling equation that uses an implicit effective length factor of K = 0.5 (AASHTO 2020). AASHTO also requires checks for block shear, net-section fracture, and shear rupture. CSA S6 follows a similar Whitmore-based approach but uses a different column-strength formulation for compression resistance (CSA S6 2019). Overall, both standards rely on simplified buckling assumptions that were originally developed for interior joints, and neither place much attention to corner joints where only a single diagonal member is connected to gusset plate, which are common in old through-truss bridges near the ends of a truss. This research addresses this gap by developing and validating advanced nonlinear finite element (FE) models capable of capturing the deformation and buckling characteristics of corner joint gusset plates. The FE modelling framework integrates geometric and material nonlinearities, realistic fastener behaviour, and geometric imperfections. It is validated using full-scale experimental findings from FHWA's Turner-Fairbank program (Mentes 2011). Following validation, two representative corner joint configurations are examined, and systematic parametric studies using different plate thicknesses are carried out.

2. Finite Element Modelling

The finite element model for this research is developed to realistically reflect the structural behaviour of gusset plate joints under the loading conditions typically observed in steel truss bridges. A nonlinear finite element (FE) model is developed using ABAQUS software (Dassault Systèmes 2022). The model incorporates both geometric and material nonlinearities. The following subsections describe the details of FE model development.

2.1 Element and Mesh Configuration

The gusset plate and splice plates are modelled with four-node shell elements (S4R), while the connected portions of the truss members are represented using shell elements near the joint and B31 beam elements along the remaining lengths to maintain efficiency. This hybrid modelling strategy allows realistic member stiffness to be maintained without excessive mesh density. The transition between shell and beam representations is achieved using multipoint constraints (MPC).

A mesh-sensitivity study confirmed that the predicted buckling modes and capacities were not affected by element size. The FE models used shell elements of about 0.5 in. thickness, which provided converged response contours.

2.2 Fasteners in FE Model

Connector elements are used to model the load transfer between the gusset plate and the connected truss members. At each fastener location, a combination of CARTESIAN and ALIGN connectors is applied to represent shear transfer, axial restraint, and the relative slip that develops in the joint. Instead of explicitly modelling bolt geometry and hole contact, the nonlinear shear-displacement behaviour of A325 bolts is captured by calibrating the connector response to the experimentally measured force-displacement curves reported by Sanborn and Stewart (2020). Moreover, an influence radius equal to the bolt-head radius is used in the FE analysis. This approach allows the

model to produce realistic bolt-group deformation and slip while maintaining computational efficiency. Fig. 1 shows the connector elements utilized in the FE model.

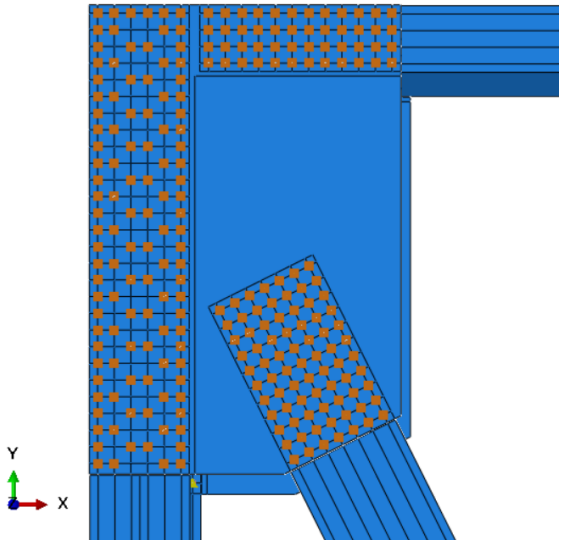

Figure 1: Connector elements used in the FE model

2.3 Boundary Conditions and Loading

Each joint is modelled as a one or two-panel truss subassembly with statically determinate and stable boundary conditions. Fig. 2 illustrates the loading and boundary conditions adopted in this study. As shown in Fig. 2, the end nodes on the outer panel perimeter (L1, L2, U2) are restrained out-of-plane, while in-plane supports are applied by restraining vertical displacement at L1 and both horizontal and vertical displacements at L2. A single out-of-plane restraint is also added at one node on the top chord outside the test joint to prevent overall out-of-plane movement of the test joint.

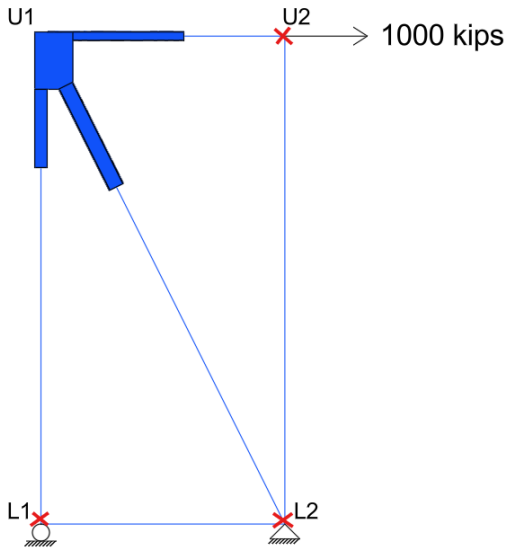

Figure 2: Typical loading and boundary conditions

2.4 Geometric Imperfection

Initial geometric imperfections were introduced through a preliminary linear analysis. Out-of-plane restraints were applied to hold all members except the compression diagonal in their ideal shape, and a small pressure load was applied to trigger the imperfection mode. The resulting displacement field was scaled to meet recommended limits: $L_{max}/150$ for plate out-of-flatness and 0.1 L_{gap} for compression diagonal out-of-plumbness (NCHRP 2013). L_{max} is the length of the longest free edge adjacent to the compression diagonal, and L_{gap} represents the shortest clear distance between the compression diagonal and adjacent members. This approach ensures that the FE model includes realistic plate and member imperfections for stability analysis.

3. Validation of Finite Element Model

The FE model is validated using the large-scale experimental testing conducted at the FHWA Turner-Fairbank Highway Research Center, as documented in the research done by Mentes (2011). The experimental configuration depicts a conventional truss-bridge connection comprising five members connected via a pair of gusset plates. These members contain a compression diagonal on the west side, a tension diagonal on the east side, a vertical member, and two chord members. The FE validation models duplicate this configuration by modelling the same member arrangement, boundary conditions, and loading sequence.

The validated FE models use the same modelling approach described in Section 2. In these models, the gusset plate, splice plates, and the near-end portions of the connected members are modelled with S4R shell elements, while the remaining member lengths are represented with B31 beam elements tied to the shell regions using MPC constraints.

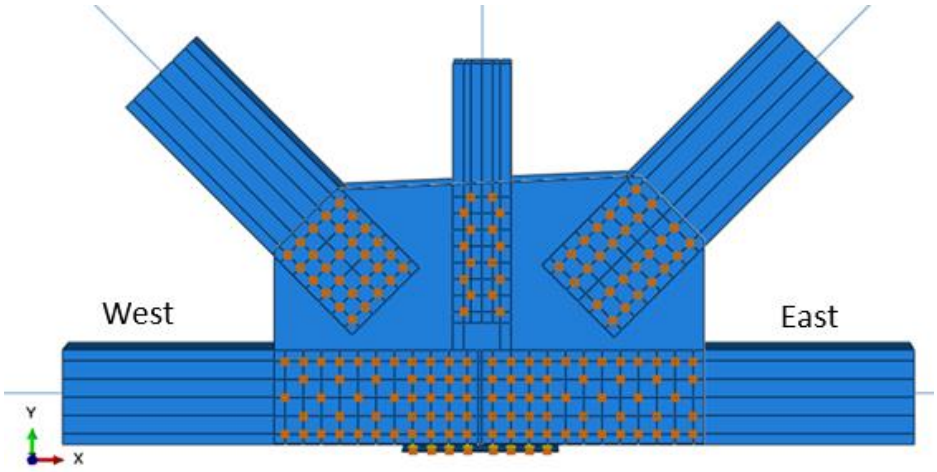

Figure 3: Assembly showing the shell elements, beam elements and connector elements used in FE models

The boundary conditions of the experimental program are replicated in the FE validation models. The west chord, shown in Fig. 3, is fully restrained and acts as the reaction chord. Axial loads are applied to the remaining four members, which are free to move solely along their longitudinal axes. Rollers are placed at the far ends of these members to permit axial movement, while torsional rotation and out-of-plane displacement are restrained to align with the experimental setup.

The experimental data is used to directly assign material properties. The connected members are expected to stay elastic during testing and are modelled using the elastic characteristics of A514

Grade 100 steel. The gusset plate represents nonlinear plate behaviour in the FE model by utilizing the true stress versus plastic strain relationship reported in the experiments (Fig. 4). To ensure realistic buckling initiation, initial geometric imperfections measured during testing are applied as out-of-plane displacements at specific nodes along the free edges and member corners.

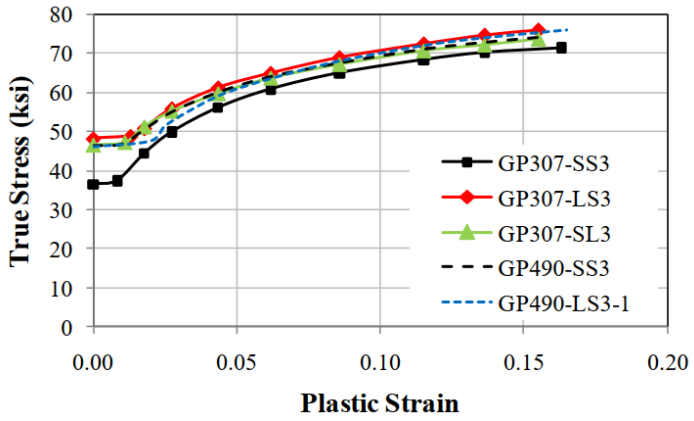

Figure 4: True stress vs. plastic strain relationship for the plate materials used in FE analysis (Mentes 2011)

Bolt behaviour is modelled using connector elements to represent the 7/8" A307 and A490 fasteners used in the experiments. The nonlinear force-displacement response of the bolts, taken from experimental shear tests (Fig. 5), is assigned to the two in-plane shear components of the connector elements.

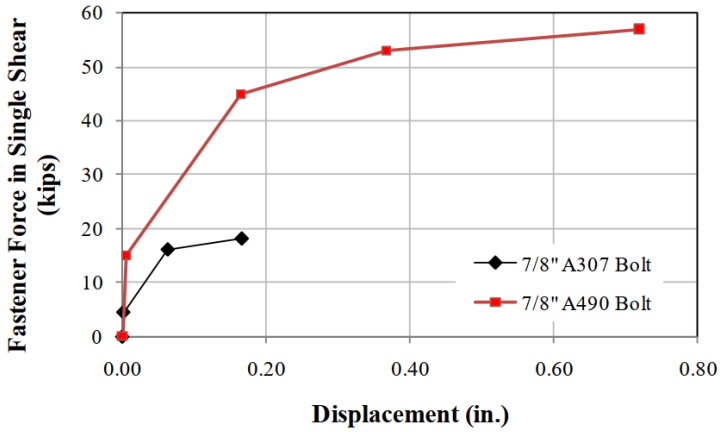

Figure 5: Fastener force vs. displacement diagram for the bolts in single shear (Mentes 2011)

3.1 Details of the Validated Specimens

The five gusset plates used to validate the FE models have a thickness of 3/8". The framing angle of the diagonal members in the test specimens was 45° in all the experiments. For each specimen, 3/8" splice plates were produced from the same plate material as the gusset plates. While FE models were developed and validated for all five configurations, only three representative specimens are presented in this paper. Fig. 6 shows the cross-section of the truss members attached to the gusset plates.

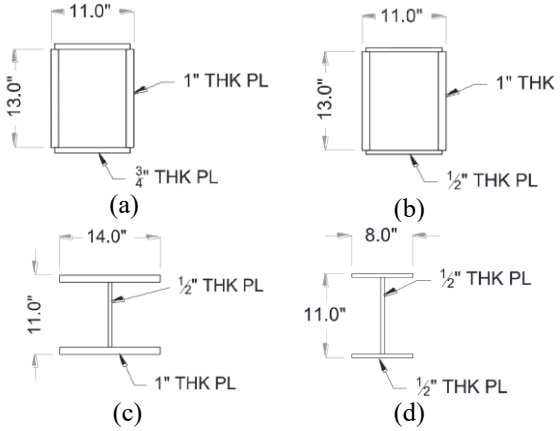

Figure 6: Cross-section of the truss members (a) east and west chord, (b) compression diagonal, (c) tension diagonal and (d) vertical member (Mentes 2011)

The following Figures present the cross-sections of the three gusset plate specimens utilized for validation. The main differences between the specimens are the length of the free edge. Specimens labeled GP307 were fastened with A307 bolts, whereas the GP490 series used A490 bolts.

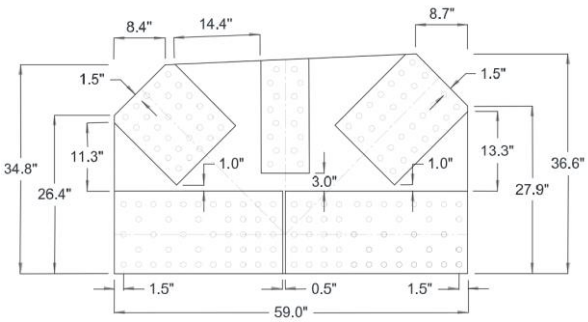

(a) GP307-SS3

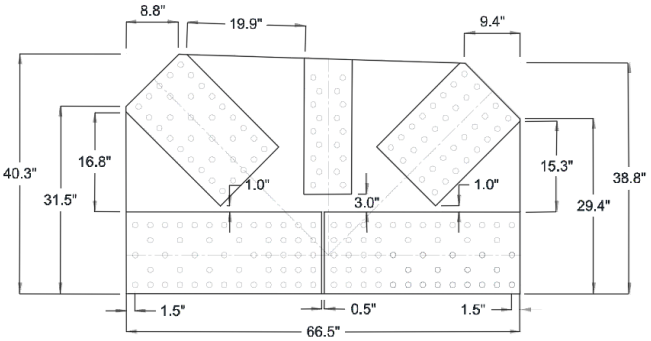

(b) GP307-SL3

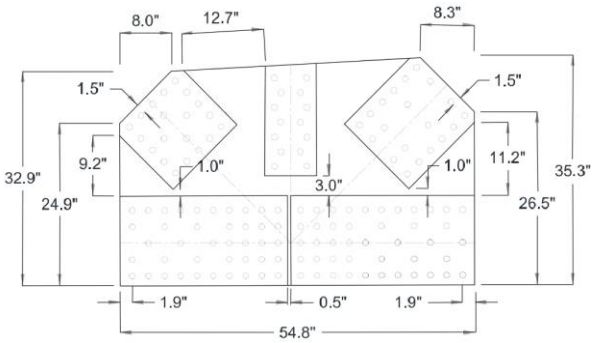

(c) GP490-SS3

Figure 7: Cross-sections of the gusset plate specimens (Mentes 2011)

3.2 Analysis of Gusset Plate Behaviour

Nonlinear FE analyses were performed to study the failure behaviour of the gusset plates. For each test, the recorded member forces at the onset of joint failure were applied to the FE models, and the corresponding load proportionality factors were extracted. Table 1 shows that the FE predictions differ from the experimental capacities by only about 0.4% to 6.7%. This close

agreement shows that the FE models capture the overall response and failure behaviour of the joints with good accuracy.

Table 1: Comparison Between Experimental Data and FE Predictions

Specimen	Truss Member	Experimental Result (kip)	FE Result (kip)	% Error
GP307-SS3	Compression Diagonal	716	718.7	0.4
	Vertical Member	-141	-141.5	
	Tension Diagonal	-507	-508.9	
	East Chord	520	522.0	
GP307-SL3	Compression Diagonal	946	953.8	0.8
	Vertical Member	0	0.00	
	Tension Diagonal	-929	-936.7	
	East Chord	706	711.9	
GP490-SS3	Compression Diagonal	728	777	6.7
	Vertical Member	0	0	
	Tension Diagonal	-728	-777	
	East Chord	538	574	

For most specimens, failure was governed by side-sway buckling of the gusset plate on the compression diagonal side. The only exception was GP307-SL3, which developed shear along the horizontal plane before exhibiting out-of-plane movement of the compression diagonal. Buckling behaviour was identified from the FE mode shapes and the load-displacement responses. As shown in Fig. 8, the GP307-SS3 model displays a substantial increase in out-of-plane displacement relative to in-plane (horizontal) displacement near the compression diagonal, confirming a buckling-controlled failure. Similar trends were observed in the remaining specimens, except for GP307-SL3. In that case, Fig. 9 indicates that horizontal displacement dominated the response, indicating a shear-driven failure mode.

As experimental displacement data were not available, the responses shown in Figs. 8 and 9 are based solely on the FE models. For GP307-SL3, plastic strains exceeded 4%, a commonly accepted threshold for the onset of significant ductile deformation in gusset plate studies. Accordingly, the load corresponding to 4% Equivalent Plastic Strain (PEEQ) was taken as the adequate capacity. For all other specimens in which PEEQ remained below this limit, the maximum load proportionality factor was used to define the capacity.

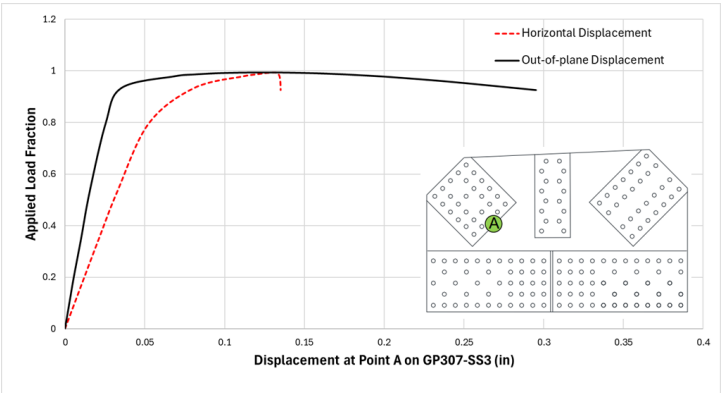

Figure 8: Comparison between in-plane (horizontal) displacement and out-of-plane displacement for GP307-SS3 specimen

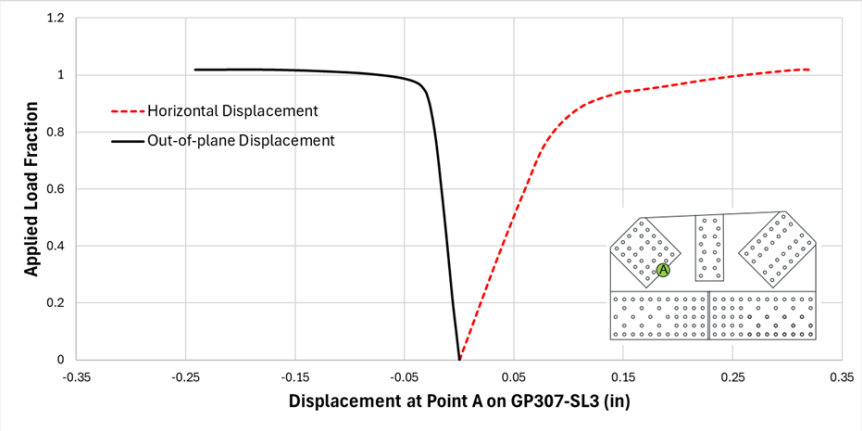

Figure 9: Comparison between in-plane (horizontal) displacement and out-of-plane displacement for GP307-SL3 specimen

Fig. 10 compares the experimentally observed failure modes reported by Mentes (2011) with the FE-predicted modes for the GP307-SS3 specimen. For the remaining specimens, similar figures have been obtained as well. In the FE stress contours, the gray region indicates the yielded areas, and the deformation scale is set to 5 for all diagrams. Overall, the FE models reproduced the observed failure mechanisms closely, reinforcing the validity of the numerical approach.

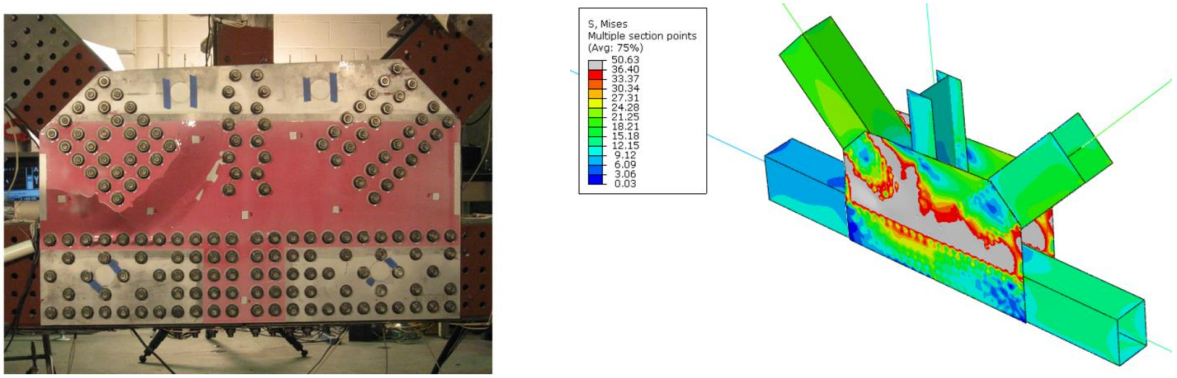

(a) (b)

Figure 10: GP307-SS3 specimen showing the buckled gusset plate (compression diagonal is on the left) (a) experiment (Mentes 2011) and (b) FE analysis

Moreover, a digital image correlation (DIC) device was used in the experimental program to assess Tresca strain on the North gusset plate. Both the DIC strain contours and the FE strain contours exhibit the tension diagonal on the left and the compression diagonal on the right, as seen in Fig. 11. Similar figures have been obtained for the rest of the specimens. Minor variations between the experimental and numerical contour patterns are likely due to the initial geometric imperfections introduced into the FE model.

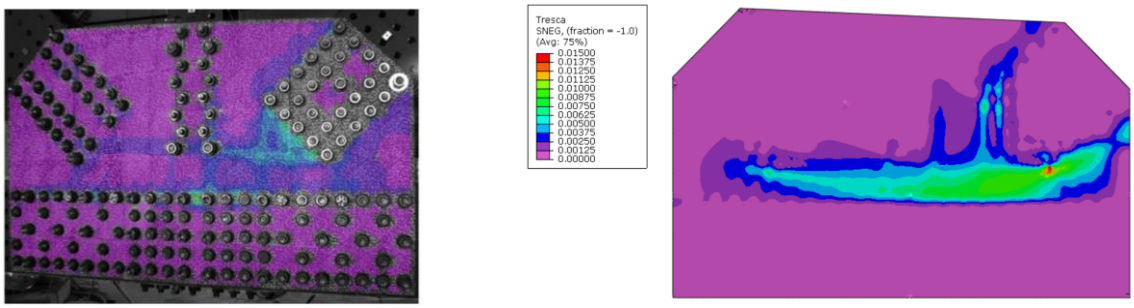

(a) (b)

Figure 11: Comparison between the Tresca strain contours obtained from (a) experiment (Mentes 2011) and (b) FE model before failure (compression diagonal on the right side) for GP307-SS3

4. Behaviour of Corner Gusset Plates

The second phase of this research focuses on the behaviour of corner joint gusset plates in steel truss bridges. Two representative corner joint geometries are selected based on typical bridge configurations (Fig.12), and the associated loading scenarios are established to reflect realistic axial forces transmitted through the connected members. For each geometry, the gusset plate layouts are designed according to AASHTO specifications. Detailed geometric representations of the gusset plates used in the study are shown in Fig. 13. To support the numerical study, a set of representative truss members is specifically designed for use in the FE analyses. The members are proportioned to prevent member-level failure, ensuring that the global response is controlled by the gusset plate and that the analysis isolates gusset behaviour.

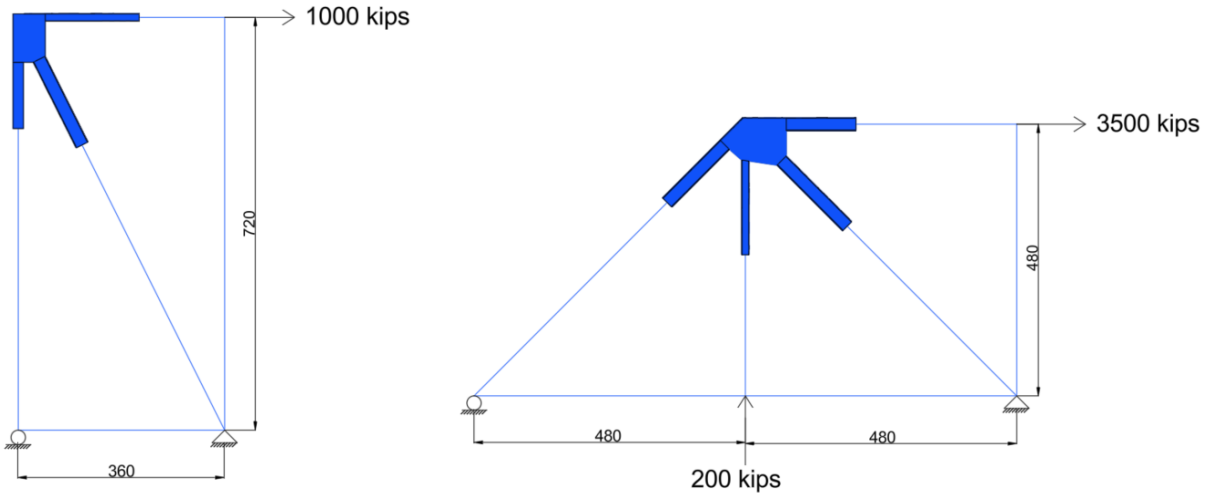

(a) Corner Joint-1 (b) Corner Joint-2

Figure 12: Summary of bridge configurations of corner gusset plate joints

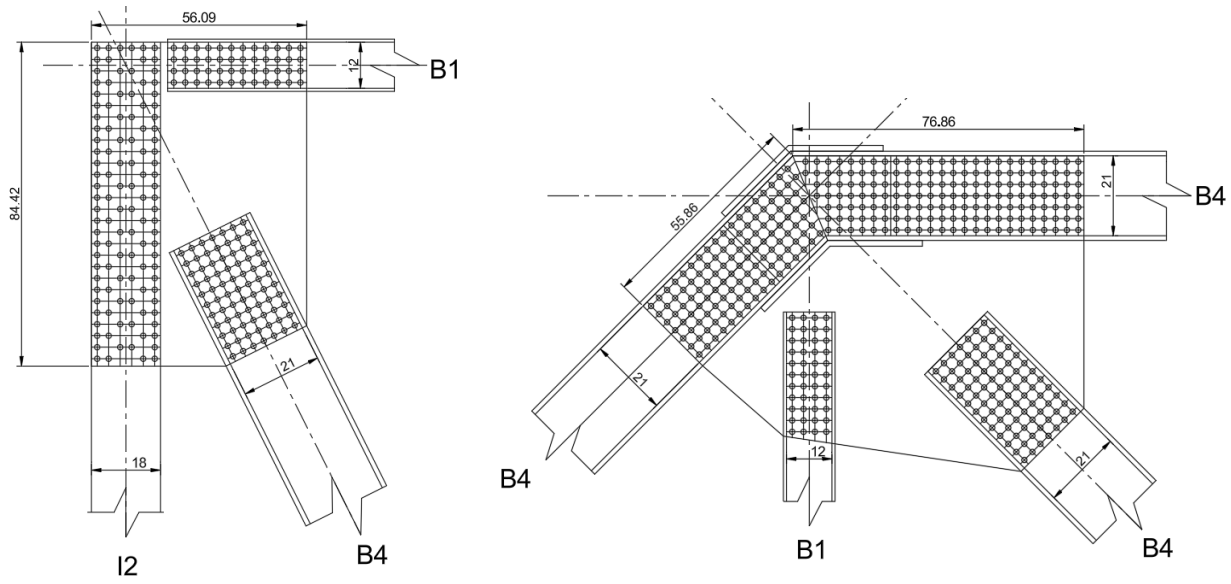

(a) Corner Joint-1 (b) Corner Joint-2

Figure 13: Gusset plate geometry

Using the modelling approach outlined in Section 2, several nonlinear FE analyses have been carried out. The connections in the corner joint models are represented using 7/8 in A325 bolts. Their behaviour is implemented through nonlinear shear force-shear displacement data reported by Sanborn and Stewart (2020) (Fig. 14), which is assigned directly to the connector elements in the FE model. The gusset plates are modelled using the true stress-strain relationship for Grade 50 steel reported in the NCHRP (2013) dataset, ensuring that the material response in the FE model reflects the same constitutive behaviour as that used in the reference physical testing. Fig. 15 shows the true stress-strain curves for Grade 50 steel.

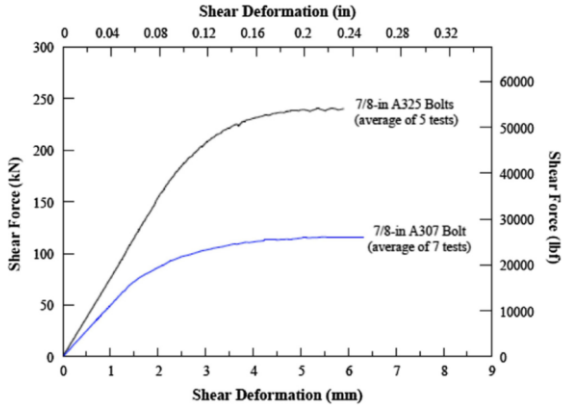

Figure 14: Nonlinear shear-force shear-displacement curve for A325 bolt in single shear (Sanborn and Stewart 2020)

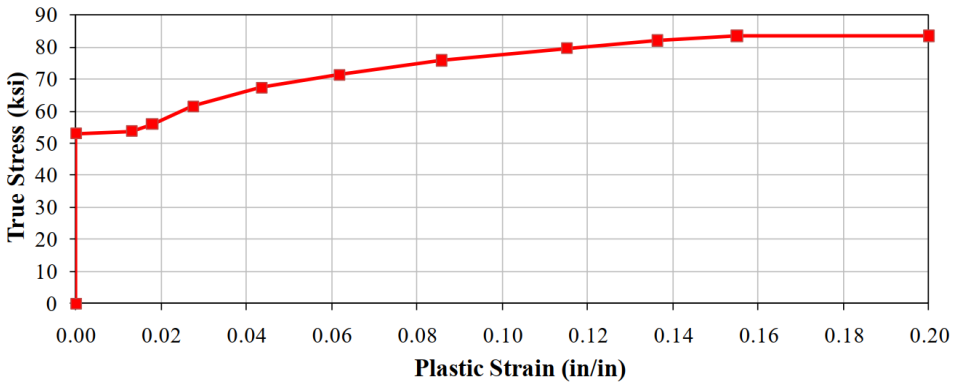

Figure 15: True stress-strain curves for Grade 50 steel (NCHRP 2013)

For each corner joint geometry, a parametric study has been performed in which the gusset plate thickness is systematically varied. In every case, the FE results showed that out-of-plane buckling governed the compressive resistance of the corner joint. Figs. 16 and 17 show the von-Mises stress contour and PEEQ contour for the two representative corner gusset plates. In the FE stress contours, the gray region represents the yielded areas. The significantly larger out-of-plane displacement compared to the in-plane (horizontal) displacement near the compression diagonal at failure confirms that the specimen failed by buckling. For all the models, PEEQ remained below 4%. In Figs. 16 and 17, t_g denotes the gusset plate thickness.

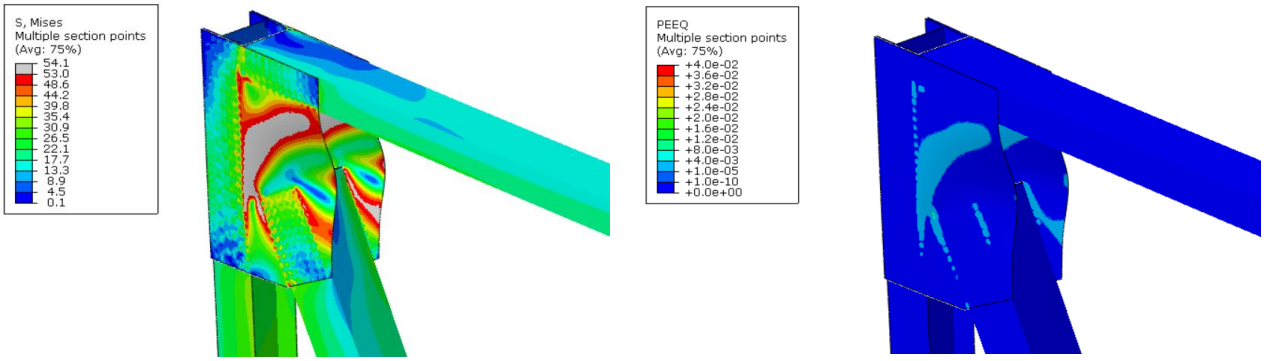

(a) (b)

Figure 16: (a) von-Mises stress contour and (b) PEEQ contour for Corner Joint-1 (t_g= 0.6 in.)

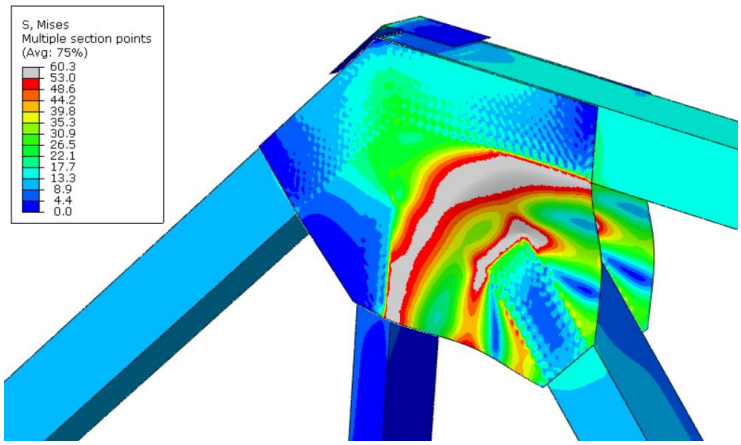

(a)

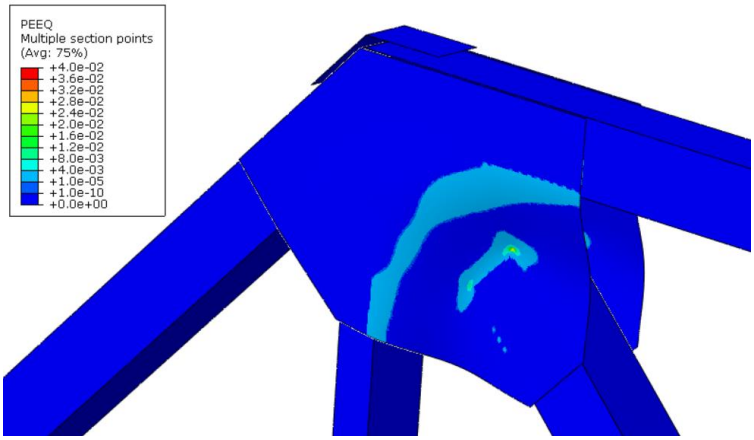

(b)

Figure 17: (a) von-Mises stress contour and (b) PEEQ contour for Corner Joint-2 (t_g= 0.6 in.)

5. Comparison with Codes

In this section, results from FE models are compared with AASHTO (2020) and CSA S6 (2019). A consistent set of symbols is used when expressing gusset plate design provisions. These include- A_g, the gross cross-sectional area; and A_{vg}, the gross shear area. Material properties are defined by the specified minimum yield strength F_y, the specified minimum tensile strength F_u, and the elastic modulus E. The gusset plate thickness is denoted as t_g.

5.1 AASHTO LRFD Bridge Design Specifications

Compression design is based on Whitmore's effective width, using a 30° dispersion angle to define A_g, as shown in Fig. 18. The nominal resistance P_n follows a column-type buckling expression using yield strength $P_o = F_y A_g$ and elastic buckling load P_e. The nominal compressive resistance is determined using the expressions provided in Eqs. 1 to 3.

If $\frac{P_o}{P_e} \leq 2.25$, then:

$$P_n = \left[0.658^{\left(\frac{P_o}{P_e}\right)}\right] P_o \tag{1}$$

Otherwise:

$$P_n = 0.877 P_e \tag{2}$$

$$P_e = \frac{3.29E}{\left(\frac{L_{mid}}{t_g}\right)^2} A_g \tag{3}$$

The column length L_{mid} is taken from the center of the Whitmore section to the nearest fastener line in the loading direction, and an implicit effective length factor K = 0.5 is assumed for all configurations.

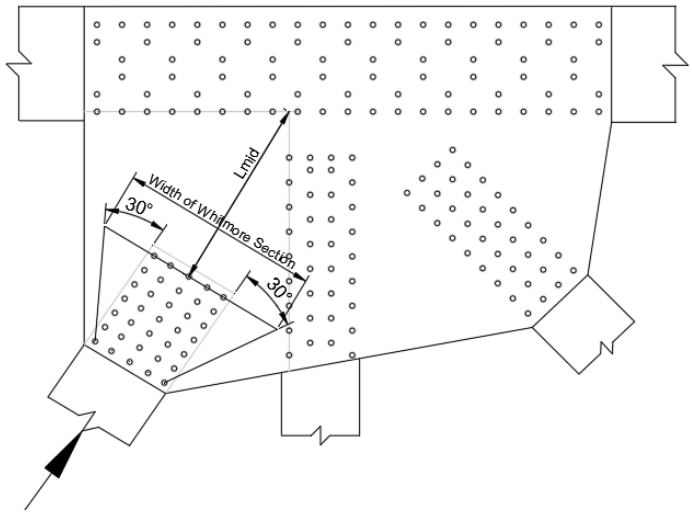

Figure 18: Connection showing the Whitmore section for a compression member derived from 30˚ dispersion angles and the distance L_{mid} (AASHTO 2020)

AASHTO further specifies that partial shear around the compression member must be evaluated using Eq. 4. In Eq. 4, shear reduction factor for gusset plates (Ω) taken as 0.88

$$V_n = 0.58 F_y A_{vg} \Omega \tag{4}$$

5.2 CSA S6 Design Specifications

CSA S6 follows a Whitmore-based approach for the gusset plate, similar to AASHTO, but uses column-strength formulation for compressive resistance as shown in Eqs. 5 and 6. In the following equations, n is taken as 1.34, the effective length factor K is 0.5, and r_g denotes the radius of gyration of the gusset plate at the Whitmore section.

$$P_n = \frac{A_g F_y}{(1 + \lambda^{2n})^{\frac{1}{n}}} \tag{5}$$

$$\lambda = \left(\frac{K L_{mid}}{r_g}\right) \sqrt{\frac{F_y}{\pi^2 E}} \tag{6}$$

5.3 Comparison of FE Predictions with Code

Fig. 19 compares the compressive resistances obtained from the FE models and from Mentes's (2011) experimental program with the predictions of AASHTO and CSA S6 across a wide range of slenderness parameters, λ_s. The slenderness parameter for the gusset plate is defined here as

$$\lambda_s = \frac{P_o}{P_e} = \left(\frac{L_{mid}}{t_g}\right)^2 \frac{F_y}{3.29\, E} \tag{7}$$

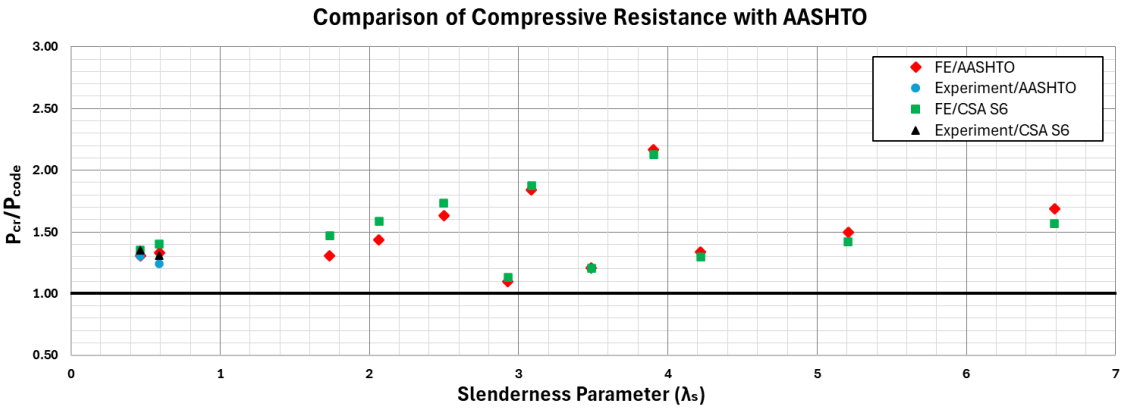

Figure 19: Comparison of FE and Experimental Capacities with AASHTO and CSA S6 Predictions

Overall, both codes underestimate the actual capacities, with most FE-to-code and experiment-to-code ratios falling between roughly 1.1 and 1.8. For slenderness values between about 0.5 and 2, the predictions remain conservative; however, CSA S6 tends to give slightly lower resistances than AASHTO, which leads to higher FE/CSA and experiment/CSA ratios in this range. As λ_s increases into the intermediate range (around 2 to 5), both FE/AASHTO and FE/CSA ratios often exceed 1.5.

Taken together, these results indicate that AASHTO and CSA S6 provide conservative estimates of compressive resistance across the entire slenderness range for the gusset plate geometries investigated. The degree of conservatism grows more pronounced at higher slenderness values, where the codes increasingly underpredict capacity due to their simplified treatment of plate buckling and effective length. The consistent trends for both FE and experimental datasets also reinforce the reliability of the validated FE models used in this study.

6. Conclusions

This study examined the compression behaviour of gusset plates in steel truss bridges through detailed nonlinear FE analysis in ABAQUS. The models included both material and geometric nonlinearities and represented realistic boundary conditions and member interactions. Five gusset plate configurations were first modelled and validated against available experimental results, demonstrating that the FE approach can reliably reproduce the observed capacities and failure modes. Three representative validation specimens are presented in this paper. Furthermore, a series of corner gusset plate connections from truss bridges was then analysed to study their behaviour under compression. The FE results consistently showed higher capacities than those predicted by AASHTO and CSA S6 across the full range of slenderness values considered. This difference is most noticeable at intermediate slenderness levels. Overall, the findings show that current code checks tend to be conservative for gusset plates in compression and may not fully represent their actual load-carrying capacity. The validated FE modelling framework developed in this study offers a reliable basis for future parametric work aimed at improving design guidance for corner joint gusset plate stability.

Acknowledgments

Funding for this research project is provided by the Canadian Institute of Steel Construction (CISC), Mitacs, and the Gina Cody School of Engineering and Computer Science, Concordia University, Montreal, Canada. The authors also thank Dr. Gilbert Y Grondin of AECOM, Edmonton, AB, Canada, for his valuable suggestions in this project.

References

American Association of State Highway and Transportation Officials (2020). "LRFD Bridge Design Specifications." AASHTO, Washington, DC.

Berman, J.W., Wang, B.S., Olson, A.W., Roeder, C.W., and Lehman, D.E. (2012). "Rapid assessment of gusset plate safety in steel truss bridges." *Journal of Bridge Engineering*, 17 (2), 221–231.

Canadian Standards Association (2019). "CSA S6:19 – Canadian Highway Bridge Design Code." CSA, Toronto, ON, Canada.

Crosti, C., and Duthinh, D. (2014). "Instability of steel gusset plates in compression." *Structure and Infrastructure Engineering*, 10 (8), 1038–1048.

Dassault Systèmes (2022). "ABAQUS/CAE User's Guide, Version 2022." Providence, RI, USA.

Duan, L., and Vinayagamoorthy, M. (2023). "Limit analysis for evaluation of compression diagonal gusset plates in steel truss bridges." *Journal of Bridge Engineering*, 28 (9), 04023056.

Federal Highway Administration (2009). "Load rating guidance and examples for bolted and riveted gusset plates in truss bridges." FHWA-IF-09-014, U.S. Department of Transportation, Washington, DC.

Higgins, C., Hafner, A., Turan, O.T., and Schumacher, T. (2013). "Experimental tests of truss bridge gusset plate connections with sway-buckling response." *Journal of Bridge Engineering*, 18 (10), 980–991.

Kim, Y.D., Mentes, Y., White, D.W., and Leon, R.T. (2013). "Analytical assessment of the strength of steel truss bridge gusset plates." *Proceedings of the Annual Stability Conference*, Structural Stability Research Council, St. Louis, MO.

Mentes, Y. (2011). "Analytical and experimental assessment of steel truss bridge gusset plate connections." Ph.D. Dissertation, Georgia Institute of Technology, Atlanta, GA.

National Cooperative Highway Research Program (2013). "NCHRP Web-Only Document 197: Guidelines for the LRFD Design and Rating of Riveted and Bolted Gusset Plate Connections for Steel Bridges, Appendix I." Transportation Research Board, Washington, DC.

National Transportation Safety Board (2008). "Collapse of I-35W Highway Bridge, Minneapolis, Minnesota." NTSB, Washington, DC.

Sanborn, M., and Stewart, L.K. (2020). "Method for evaluating impulsive shear and residual capacity behavior of bolted connections." *Engineering Structures*, 220, 110372.

Thornton, W.A. (1984). "Bracing connections for heavy construction." *Engineering Journal*, American Institute of Steel Construction, 21 (3), 139–148.

Whitmore, R.E. (1952). "Experimental investigation of stresses in gusset plates." University of Tennessee, Knoxville, TN.